The Mystery of Sub-Picosecond Charge Transfer Following Irradiation of Hydrated Uridine Monophosphate

Aurélien de la Lande, Sergey Denisov, Mehran Mostafavi

SUPPLEMENTARY INFORMATION

Figure S1: repetitions of RT-TD-ADFT electron dynamics simulations upon collision with 0.1 He2+ with thress basis sets.

Figure S2: QM/MMpol potential energy variation of the molecular system upon irradiation.

Figure S3: repetitions of RT-TD-ADFT electron dynamics simulations upon collision with 0.1 He2+ (conditions CU1 and CU2, see main text) for eleven geometries.

Figure S4: Set of localized MOs selected to be depopulated at the beginning of RT-TD-ADFT simulations A to D.

Figure S5: Charge variations with respect to the ground state of U (green), S (red), P (orange) and solvation shell (blue) after sudden depopulations of selected Kohn-Sham orbitals.

Figure S6: Fluctuations of the diabatic energy gaps calculated at the cDFT/MMpol/Onsager level of calculation along MD simulations

Figure S7: Radial distribution functions of water oxygen atoms around the USP phosphate atom.

Figure S8: Marcus free energy profiles for each 11 replicas.

Figure S9: BH&HLYP/cDFT electronic coupling time series and probability distributions.

Figure S10: vertical gap (left) and electronic coupling (right) variations upon nuclear relaxation of the system on the (US)$^+$P potential energy surface

Charge migrations after sudden ionization approximation

Calculation of Marcus free energy curves

Calculation of statistical uncertainties

ET transfers time from mean first passage

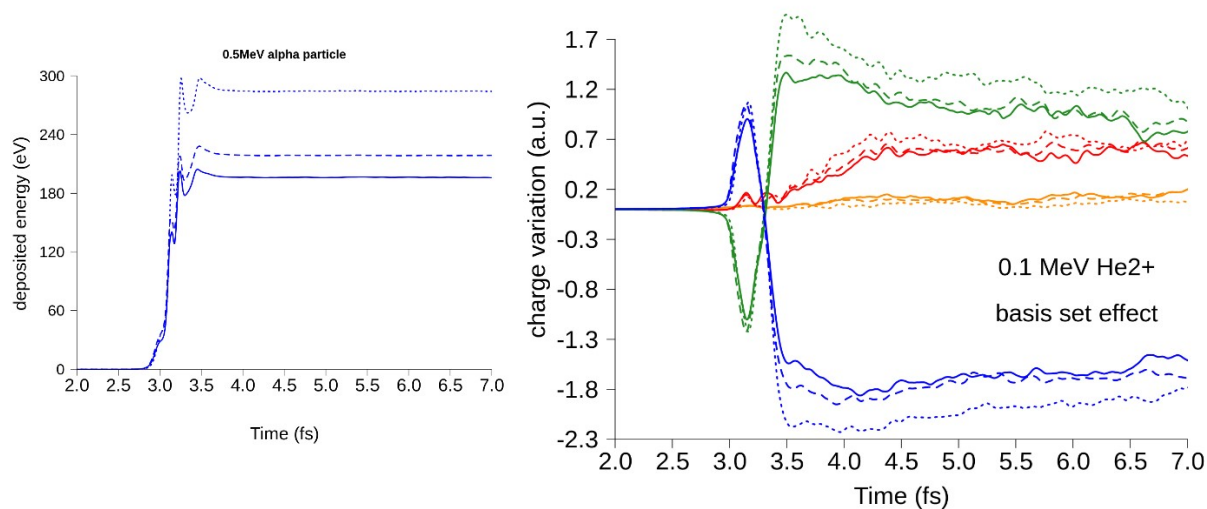Data and Rstudio Script: DOI 10.5281/zenodo.4290681

Figure S1: left, energy deposition upon collision with 0.5 He²⁺ ions with three basis sets. Right, charge variations with respect to the ground state of U (green), S (red), P (orange) and solvation shell (blue) upon irradiation by 0.5MeV He²⁺. Charge variations are calculated taking the ground state electron density as reference and using the Hirshfeld partition scheme to define atoms in molecules. BS1: DZVP-GGA on all atoms and aug-cc-pVDZ on oxygen water atoms (plain lines). BS2: TZVP on all atoms and aug-cc-pVDZ on oxygen water atoms (dashed lines). BS3: cc-pVQZ on all atoms and aug-cc-pVDZ on oxygen water atoms (plain lines).
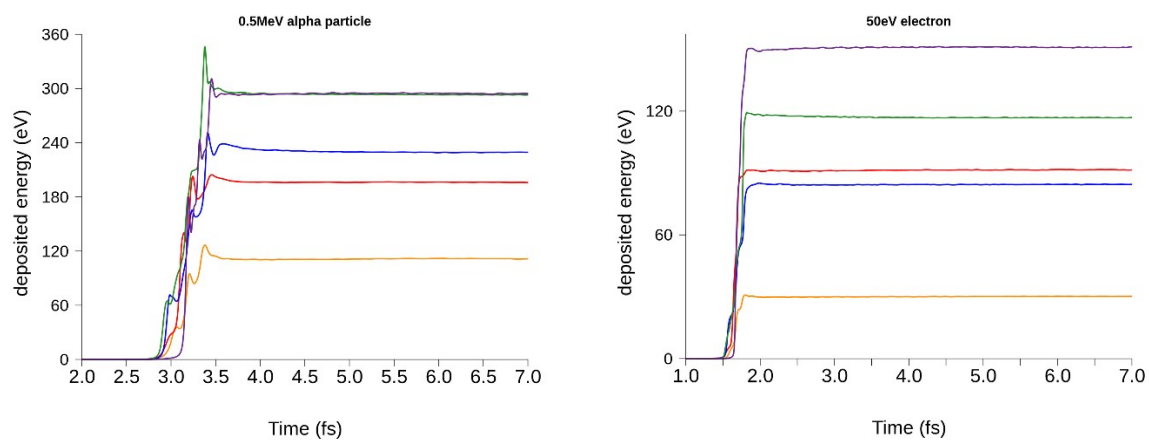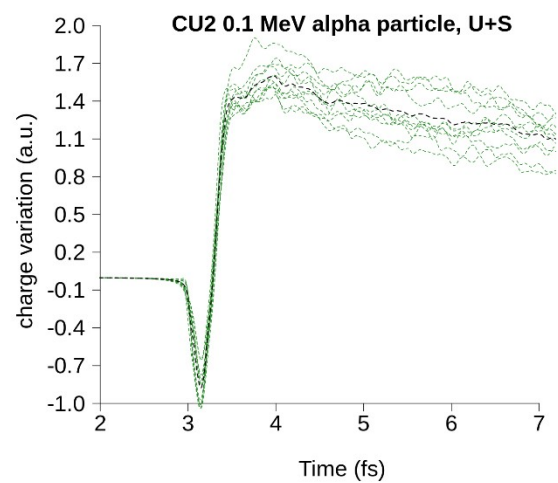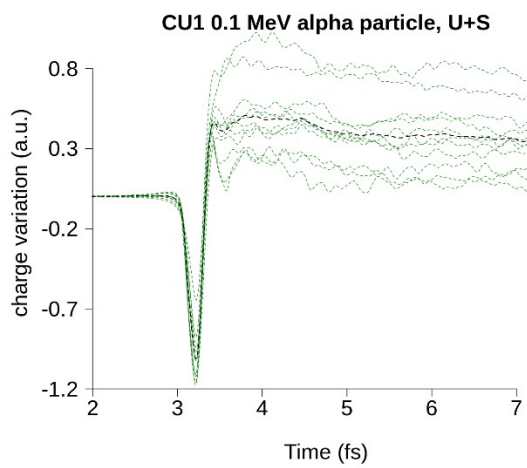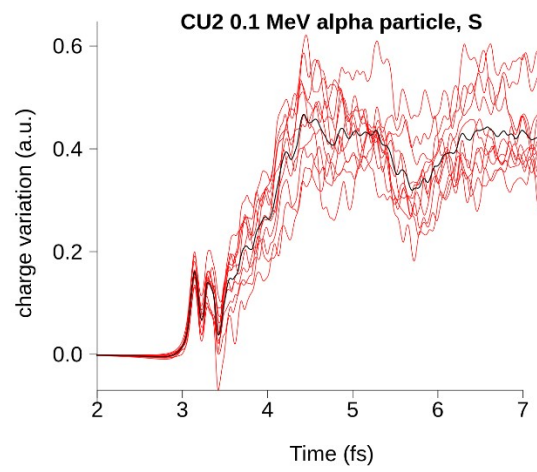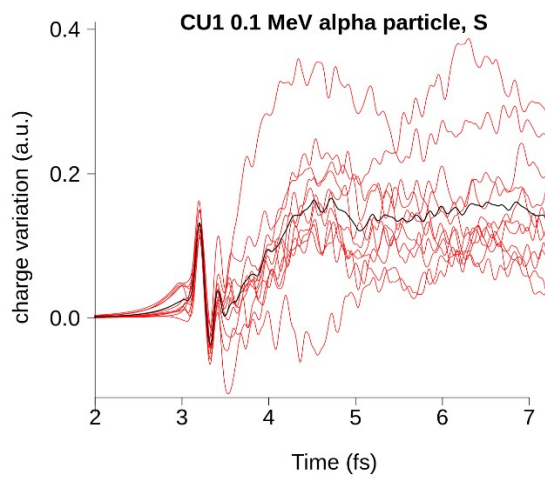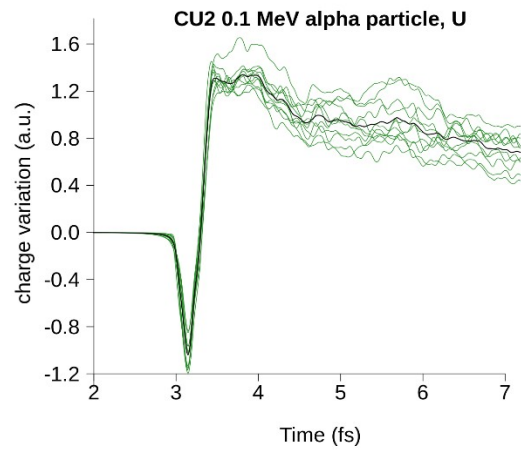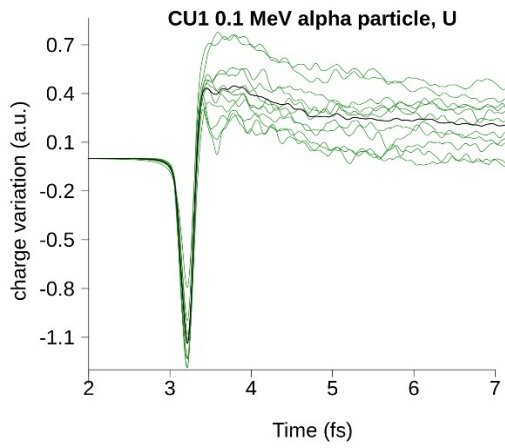
Figure S2: QM/MMpol potential energy variation of the molecular system upon irradiation by 0.1 MeV He^{2+} ion (left) or 50 eV electron (right), with respect to the ground state. Color code: CU1 trajectories in yellow, CU2 trajectories in red, trajectories CS in blue, trajectories CP in green and trajectories CW in violet.
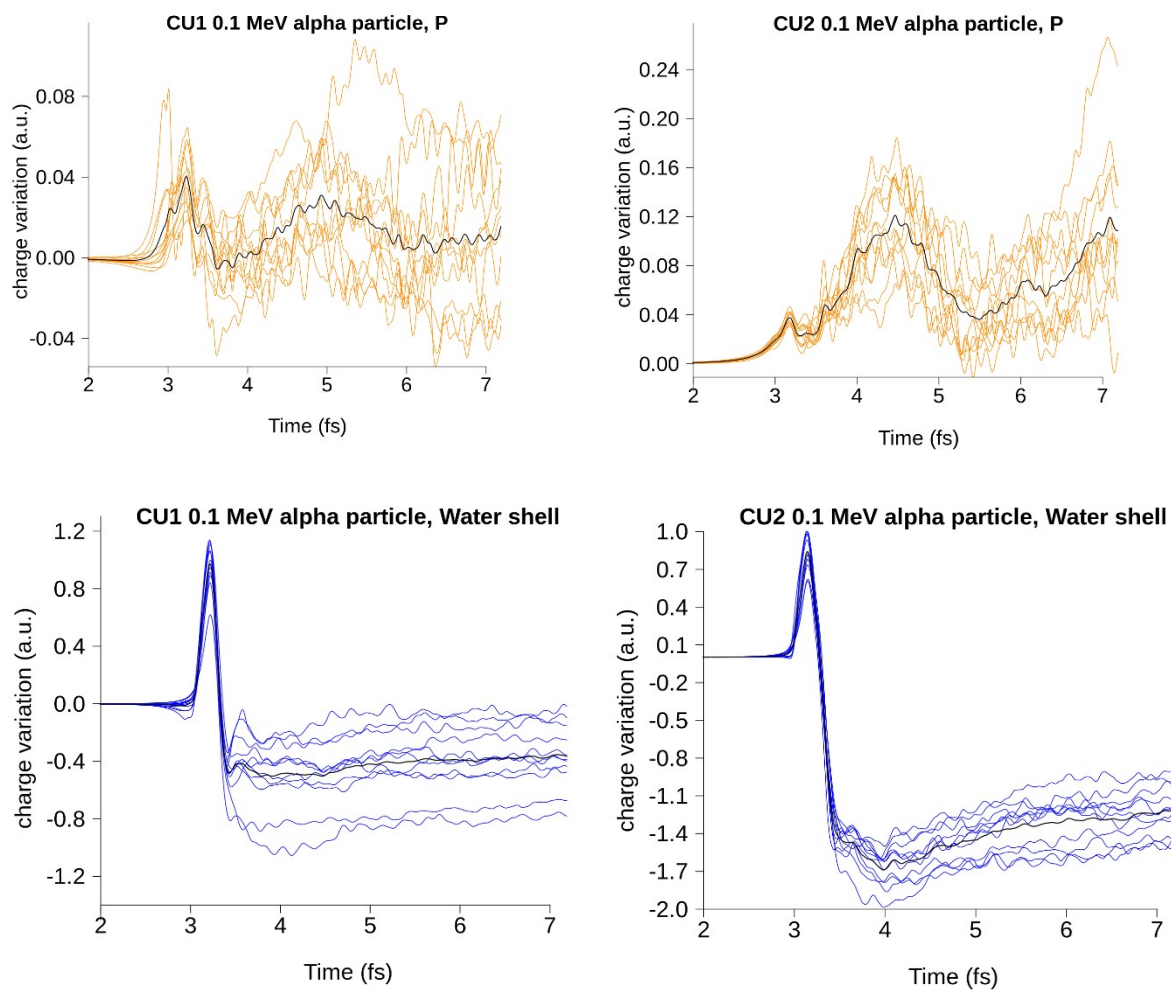
Figure S3: repetitions of RT-TD-ADFT electron dynamics simulations upon collision with 0.1 MeV He2+ (conditions CU1 and CU2, see main text) for eleven geometries of solvated USP extracted from Born-Oppenheimer MD simulations. Each color corresponds to different molecular moieties (U in green, S in red, P in dark orange, the water shell in blue). The black curves correspond to the averages.

Charge migrations after sudden ionization approximation

We start by analyzing results obtained with the first protocol consisting of depopulating Kohn-Sham MO from the SCF solution. The selected localized MOs are depicted on Figure S4. Simulations A, B, C and D, are respectively analogous to the CU1, CU2, CS and CP trajectories described above. In simulation A, we partially depopulate two π MO from the uracil base, imposing a population number of 1.5 each (we work with the restricted Kohn-Sham formalism, *i.e.* all other MOs have occupation numbers of 2.0 at the end of the SCF). In simulation B, C and D, we depopulate a σ bonding MOs of the uracil C2-N3 bond, of the ribose $C^{4'}$-$O^{4'}$ or of phosphate P-$O^{5'}$ bond respectively (see Figure 1 in the main text for atoms labelling).

The charge evolution of the U, S and P groups and of the water solvation shell are shown in Figure S5, taking the ground state charges (i.e. before ionization) as reference. In simulation A, as expected, the charge on U is close to 1.0 at time zero. It rapidly decays to 0.6 within a few tens of attoseconds and then decays almost constantly to reach a value of 0.3 at 1.5 fs. Conversely the electric charge on sugar increases. This indicates a delocalization of the hole over the entire U+S subsystem, as already described above. Nonetheless, the total charge on U and S (green-red dashed line) globally decays over a few femtoseconds at the expense of a charge increase of the solvation layer. The charge on the phosphate group, on the other hand, only marginally increases. We obtain similar trends with simulation B, except that the total U+S charge remains rather constant at 0.8 after 0.25 fs. This is probably a result of a weaker coupling between the depopulated MOs lying on the U+S moieties and MOs lying on the solvation water as compared to simulation A. In simulation C, the hole is produced on the sugar group at time zero. However, as in simulations A and B, it rapidly delocalizes over the solvation layer within 200 as, and, on a femtosecond time scale, over the entire U+S system. We find again that no hole displacement toward the phosphate group. In simulation D the hole is localized on the phosphate group. The hole delocalizes over the water layer within less than 100 as, and also over the U+S parts of the USP molecule.
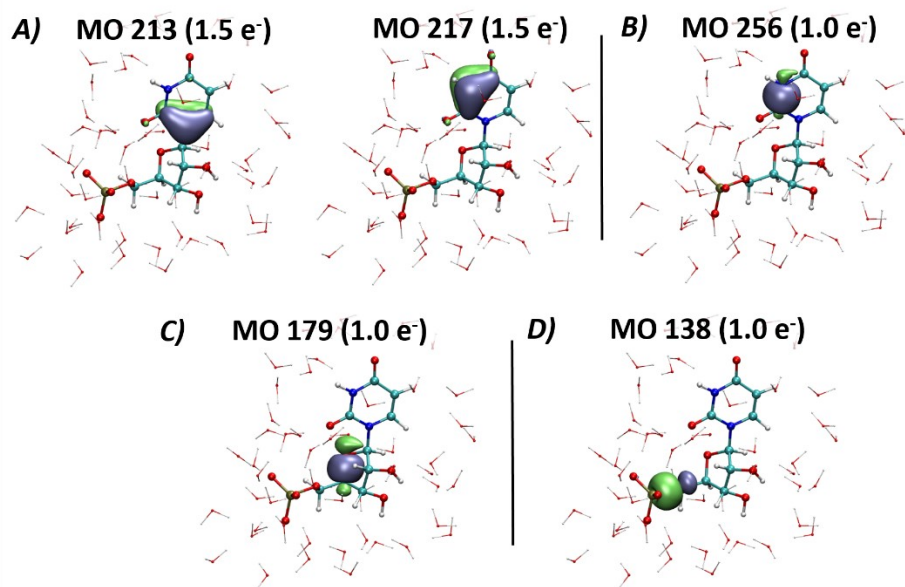
Figure S4: Set of localized MOs selected to be depopulated at the beginning of RT-TD-ADFT simulations A to D. For each simulation, the numbers in brackets indicate the population numbers of depopulated MO at time zero. For clarity, only atoms pertaining to the QM region are shown, the remaining solvent molecules are described by the POL3 model.
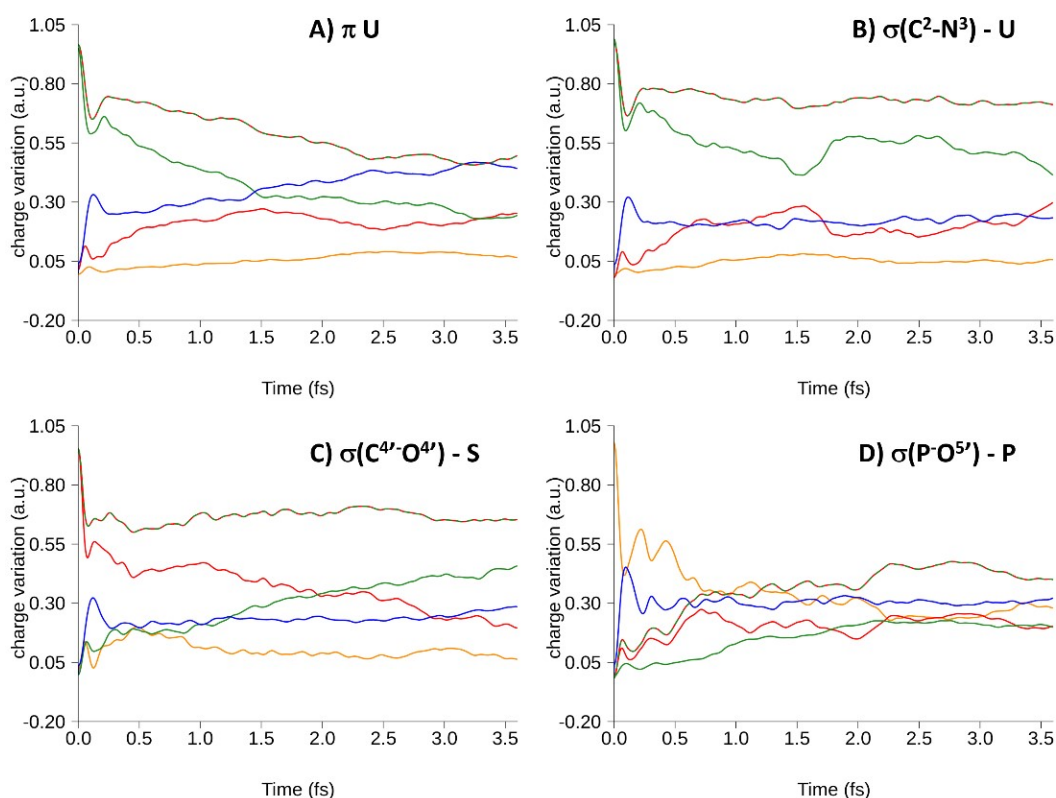
Figure S5: Charge variations with respect to the ground state of U (green), S (red), P (orange) and solvation shell (blue) after sudden depopulations of selected Kohn-Sham orbitals. Charge variations are calculated taking the ground state electron density as reference and using the Hirshfeld partition scheme to define atoms in molecules. The green dashed lines correspond for each simulation to the sum of the charge variations of U and S. The four graphs correspond to RT-TD-ADFT simulations after depopulations of the MOs depicted on Figure S4.

Marcus free energy profiles

Technical details on BOMD simulations with cDFT/MM

We refer the reader to the deMon2k manual in case of doubts about the technical terms used in the following paragraphs:

http://www.demon-software.com/public_html/support/htmlug/index.html

Born-Oppenheimer Molecular Dynamics simulations were carried in three steps. First, we generated MD trajectories on the resting state (i.e. before radiolysis) for 40 ps. We used the DZVP-GGA atomic basis set combined to the automatically generated GEN-A2 auxiliary basis. We chose the PBE functional to evaluate exchange-correlation effects by numerical integration over a grid 10^{-5} Ha accuracy (this value refers to the accuracy on the diagonal elements of the XC potential matrix). MD simulations in the NVT ensemble was achieved using a Berendsen thermostat with a system-bath coupling of 0.1ps and a temperature of 300 K. We used a velocity Verlet propagator to evolve the nuclear degrees of freedom with a timestep of 1 fs. To prevent diffusion of water molecules within the polarizable continuum (see Figure 1), all atoms situated between 30 and 33 Å away from the center of mass of the USP molecule were restrained to their initial positions by application of harmonic potentials with a force constant of 100 kJ/Å^2.

In a second step, we switched to a cDFT/MM methodology to carry out BOMD on charge transfer states. We switched to the BH&HLYP functional using a grid of fine accuracy (10^{-7} Ha). This choice of functional was motivated by the better convergence properties of BH&HLYP compared to GGA functionals. We defined charge constraints according to the Hirshfeld partitioning scheme. The cDFT weight matrix elements were obtained by numerical integration over a fixed grid of fine accuracy. The Lagrange multipliers were updated at every Self-Consistent-Field iteration with a convergence of 10^{-4} e-. cDFT/MM MD simulations were conducted for 5ps, saving geometries every 10 fs, for each of the two diabatic states.

In the third step, we reprocessed all the cDFT/MM MD trajectories to evaluate the vertical energy gap and the electronic coupling between the cDFT/MMpol diabatic states. The reprocessing step was carried out with the polarizable POL3 water model. To alleviate the risk of too frequent SCF convergence issues, we followed a strategy which is common in the literature and that consist in first carrying our SCF without updating MM induced dipoles, while optimizing induced dipoles at convergence with the Hirschfeld charges on QM atoms. This approach misses a fraction of the induction energy steming from the interplay between QM region polarization and MM region polarization, but it is expected to capture most of induction energy. When reprocessing the trajectories at the cDFT/MMpol level, the SCF sometimes

failed to converge (4% of all single point calculations). In these cases, the snapshots were discarded.

Building free energy curves

The Marcus free energy curves for the initial and final electron states, a_i and a_f respectively, are calculated by a Landau formula:

$$a_x(\varepsilon) = -\beta ln(p_x(\varepsilon)) + A_x^0$$

where ε is the reaction coordinate which is taken to be the vertical potential energy gap between the diabatic state; $p_x(\varepsilon)$ is the probability for the vertical energy gap to have a value of ε when the system samples molecular conformations of state x. A_x^0 is the absolute free energy of the system in the electronic state x. We have used the rstudio program to build all free energy curves. The scripts for the R package are provided in Supplementary materials together with the data provided by deMon2k. Briefly, we first constructed the probability histogram of the diabatic energy gaps, discarding bins containing less than two elements. The bin size was set to 0.01 eV. Each sample contained initially 4,900 snapshots. The free energy was calculated from these distributions. We then operated a linear fit to parabolic curve, assigning larger weights to the bins containing larger number of points. The fitting was carried out for each diabatic states considering both the data points coming directly from the simulation of state i, and from the application of the rule that $\Delta A = \Delta \varepsilon$ for ergodic systems.
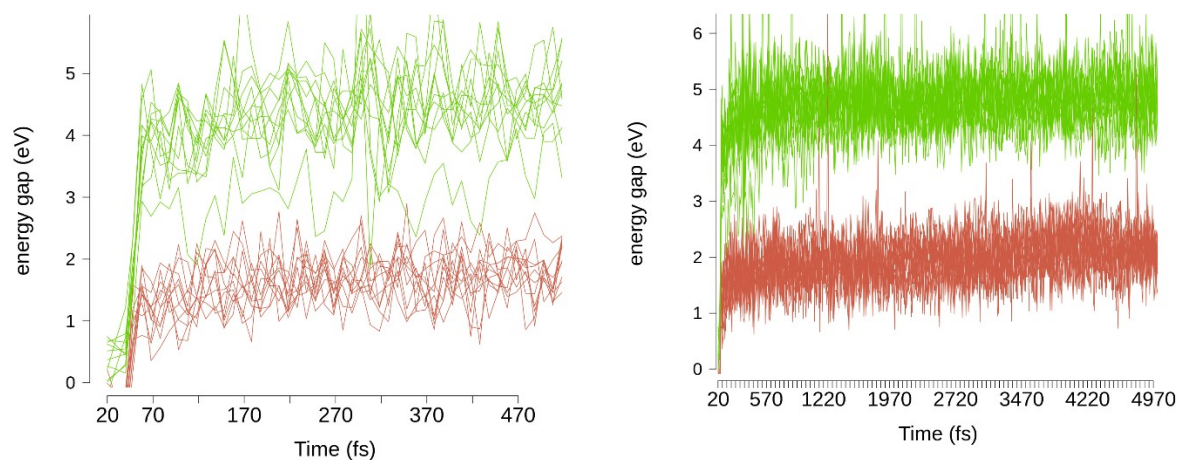

Figure S6: Fluctuations of the diabatic energy gaps calculated at the cDFT/MMpol/Onsager level of calculation along MD simulations conducted on the potential energy surfaces for the (US)+P2- and (US)P- charge transfer states (in red and green respectively).
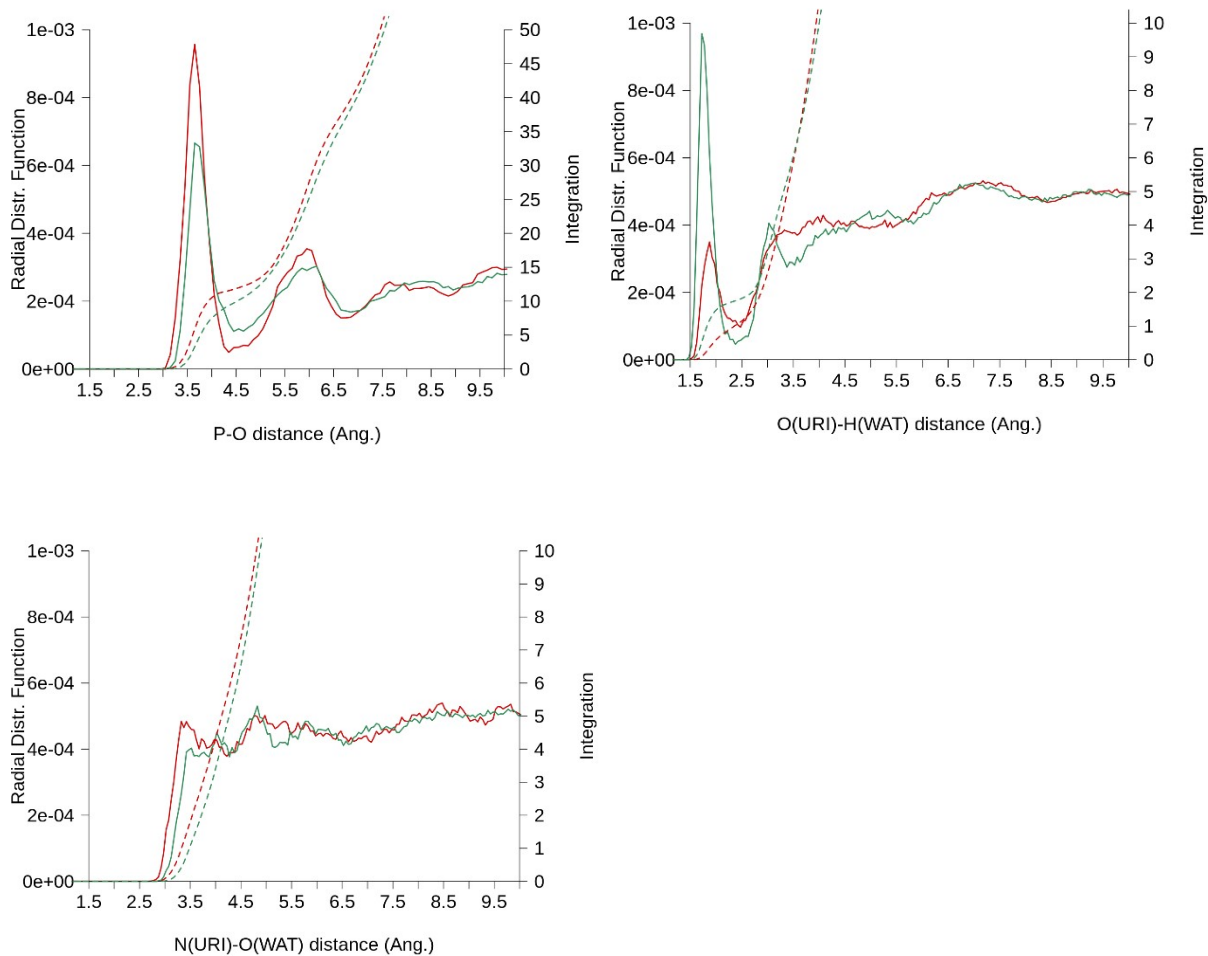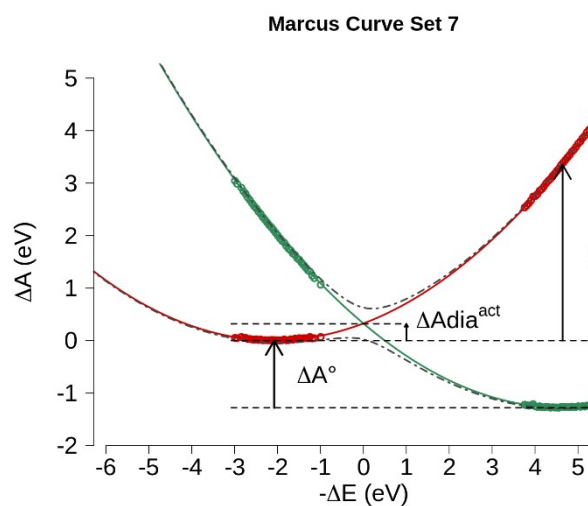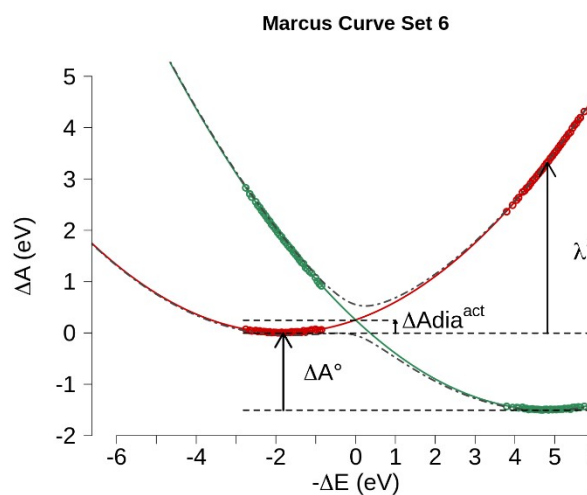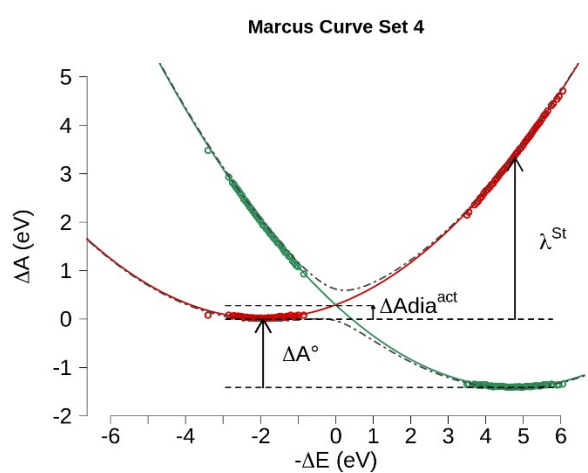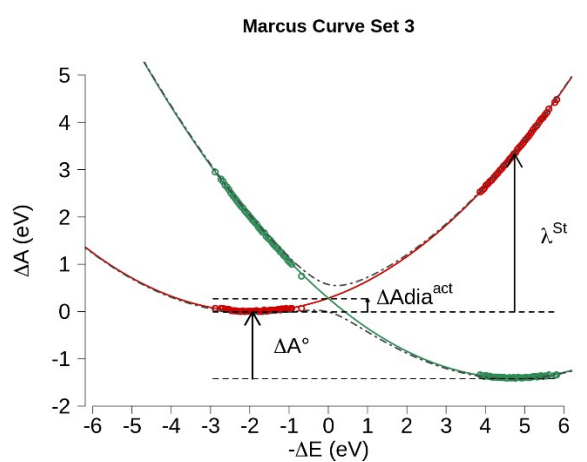
Figure S7: Radial distribution functions illustrating the reorganization of solvent around the USP molecule. The red and green curves correspond to the (US)$^+$P^{2-} and to the (US)P$^-$ diabatic states respectively. Plain curves correspond to the radial distribution functions and dashed lines correspond to the integrated RDF. The RDF were computed gathering snapshots over the last 3ps of all cDFT/MD simulations. Top-left: RDF of water oxygen molecules around the phosphate. Top-right: RDF of water hydrogen atoms around O2 and O4 oxygen atoms of the nucleobase. Bottom-left: RDF of oxygen water atoms around N3 nitrogen atom of the nucleobase. Bottom-right: water oxygen atoms

Marcus Curve Set 1

Marcus Curve Set 2

Marcus Curve Set 3

Marcus Curve Set 4

Marcus Curve Set 6

Marcus Curve Set 7
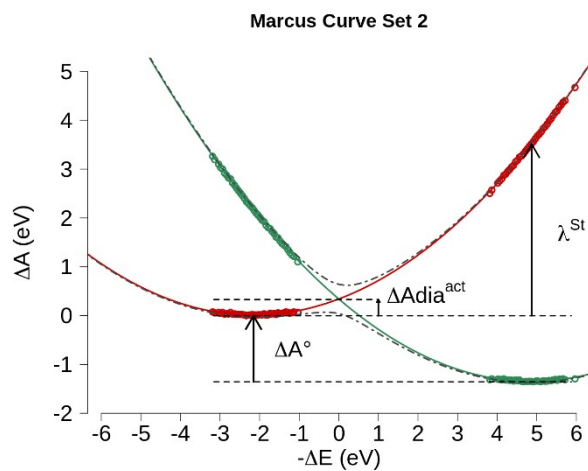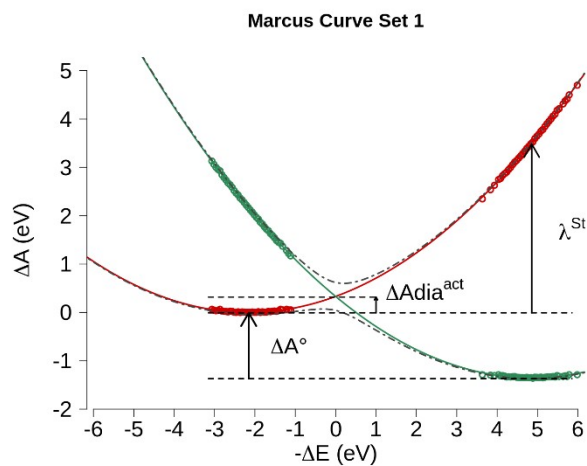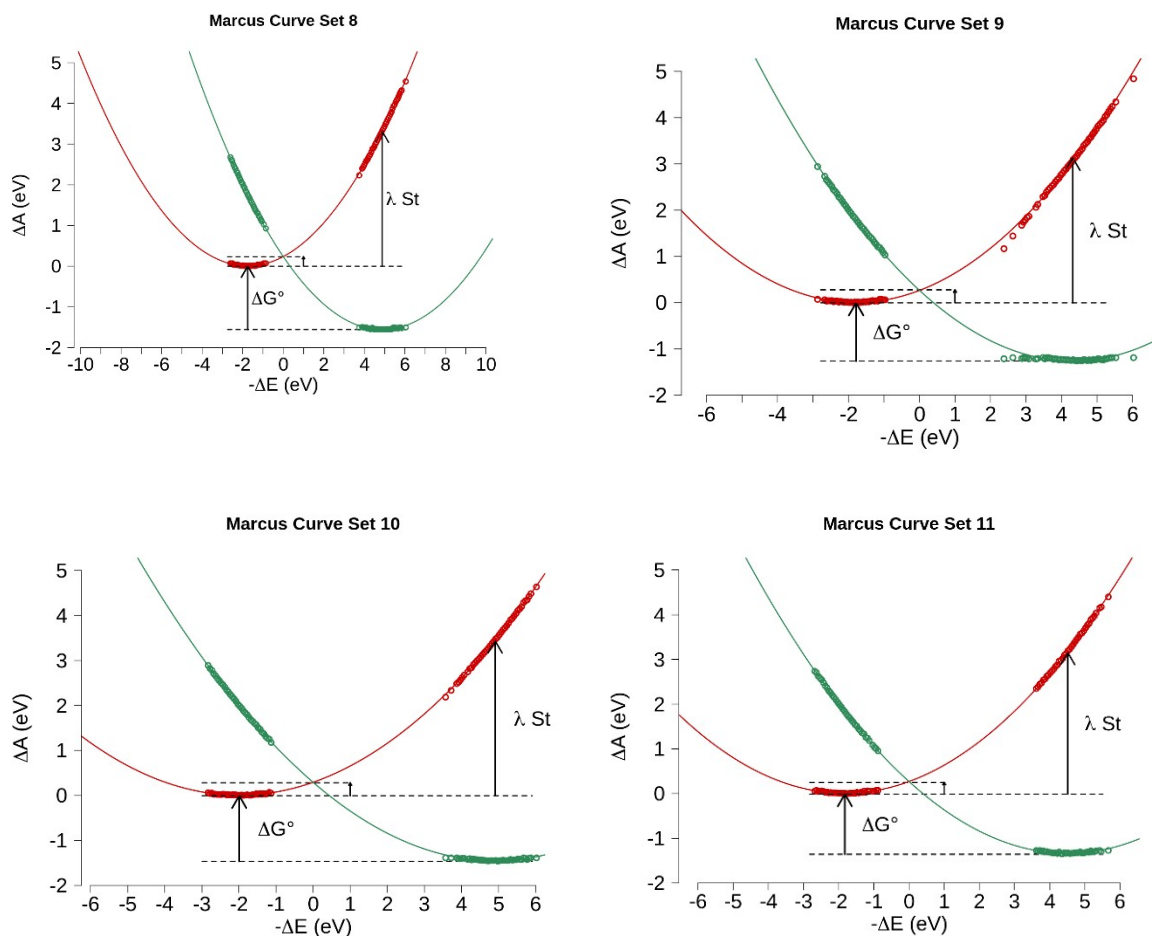
Figure S8: Marcus free energy curves for the electron transfer involving the (US)$^+$P^{2-} and (UP)P$^-$ diabatic states (initial and final states, shown in red and green, respectively). The curves have been obtained by a linear fit to a parabola, considering all the data points from 100fs to 5 ps, and considering the system to bi ergodic.

Figure S9: Electronic coupling calculated with the BH&HLYP XC functional along cDFT/MM MD simulations on the potential energy surfaces of the (US)$^+$P^{2-} and to the (US)P$^-$ diabatic states (in red and green repectively). Left: time series of electronic coupling. Right: probability distribution.

Figure S10: vertical gap (left) and electronic coupling (right) variations upon nuclear relaxation of the system on the (US)⁺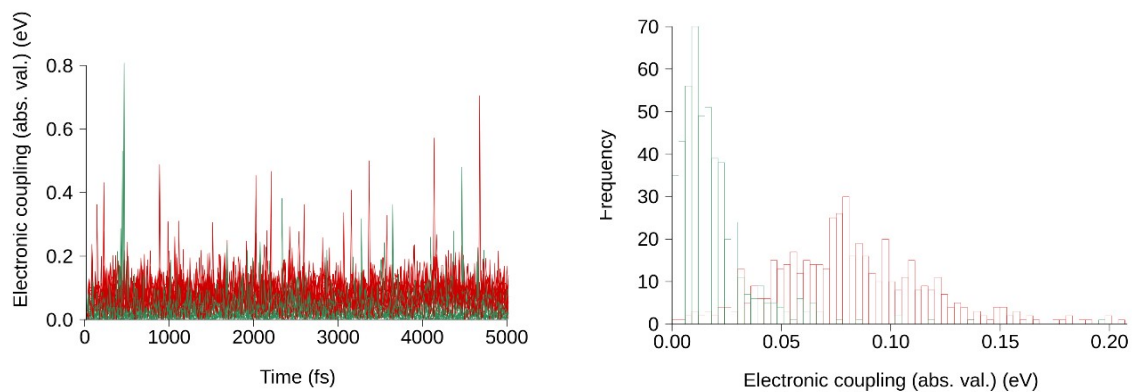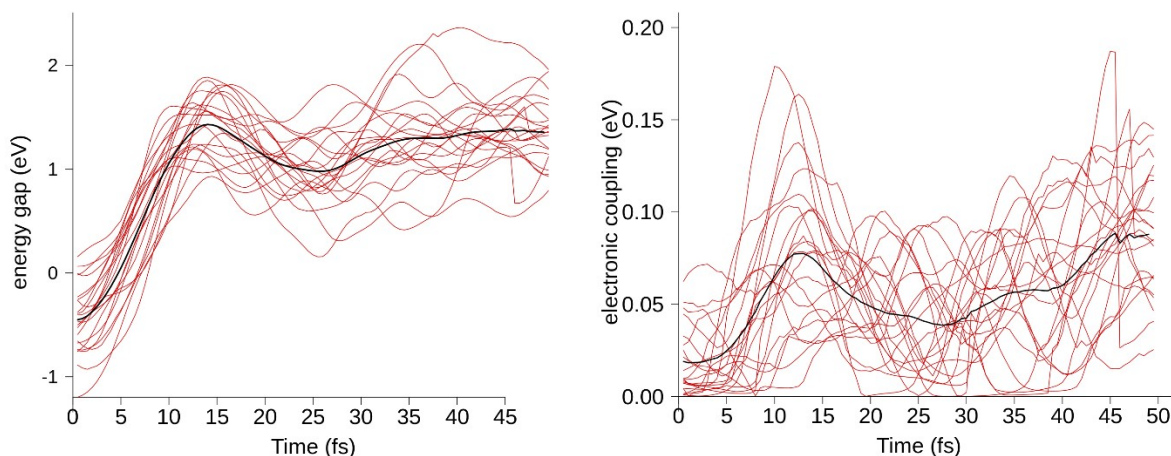P potential energy surface (i.e. subsequent to ionization). The black curve corresponds to the average over the 21 replicas. The PBE50 functional is used (raw data are available in SI for other functionals).

Calculation of statistical uncertainties

Reaction free energy and Stokes reorganization energy

Each quantity is evaluated for each run (11 in total) from the average vertical energy gap sampled from on the potential energy surface of the initial and final redox states. Knowledge of each contribution is associated to various sources of uncertainties, namely the choice of the energy function (DFT XC functional, basis set, QM/MM technique,); of the computation protocol or of the sampling method. We have evaluated from statistical uncertainties due to the sampling method.

For a pair of QM/MM MD trajectories in electronic states *i* and *f*, the uncertainties of ΔA° and λ^{St} are computed using propagation uncertainty formula, from the variance of the mean vertical energy gaps $\langle \Delta E \rangle_i$ and $\langle \Delta E \rangle_f$ along the two trajectories:

$$u^2(\Delta A^\circ) = u^2(\lambda^{St}) = \frac{1}{4}\left(u^2(\langle \Delta E \rangle_i) + u^2(\langle \Delta E \rangle_f)\right)$$

The variance of the mean energy gaps is obtained from the dispersion of the energy gap along the simulation:

$$u^2(\langle \Delta E \rangle_x) = \frac{var(\Delta E)_x}{\rho_x N_x}$$

Where N_x and ρ_x are the number of points sampled along the simulation x and the chain efficiency of the MD simulation. The latter quantity has been obtained from the energy gap

auto-correlation function using the effectiveSize procedure of the coda package of the R software. This leads to:

$$u^2(\Delta A^\circ) = u^2(\lambda^{St}) = \frac{1}{4}\left(\frac{var(\Delta E)_i}{\rho_i N_i} + \frac{var(\Delta E)_f}{\rho_f N_f}\right)$$

Variance reorganization energy

For each simulation (in electronic states *i* and *f*), we have computed the reorganization energy from the variance of the energy gap ΔE, according Eq. 5 of the main text:

$$\lambda^{var}_x = \frac{\beta.var(\Delta E)_x}{2}$$

Uncertainty on each individual λ^{var}_x value is estimated through

$$u^2(\lambda^{var}_x) = \frac{\beta^2}{4}\frac{2(var(\Delta E)_x)^2}{\rho_x N_x}$$

Electron transfer characteristic times

The characteristic ET times in the context of the non-adiabatic Marcus (NAM) Theory have been evaluated as the inverse of the non-adiabatic rate constant:

$$\tau^{NAM}_{ET} = \frac{\hbar\sqrt{4\pi/\beta}}{2\pi}.\frac{\sqrt{\lambda^{St}}\exp\left(\beta\Delta A^{\neq}\right)}{\langle H^2_{DA}\rangle}$$

Propagations of the statistical uncertainties on each of the $\Delta A^{\neq}$, $\langle H^2_{DA}\rangle$ and λ^{St} to the evaluation of τ_{ET} have been estimated from uncertainty propagation formulas. If a function y depends on three parameters, a,b and c ($y = f(a,b,c)$) associated to uncertainties $u^2(a)$, $u^2(b)$ and $u^2(c)$, then the maximal uncertainty on y is given by:

$$u^2(a) = \left|\frac{\partial y}{\partial a}\right|u^2(a) + \left|\frac{\partial y}{\partial b}\right|u^2(b) + \left|\frac{\partial y}{\partial c}\right|u^2(c)$$

Therefore, in the case of τ^{NAM}_{ET} we find:

$$u^2(\tau^{NAM}_{ET}) = C\left[\frac{\sqrt{\lambda^{St}}}{\langle H^2_{DA}\rangle^2}u^2(\langle H^2_{DA}\rangle) + \frac{1}{2\langle H^2_{DA}\rangle\sqrt{\lambda^{St}}}u^2(\lambda^{St}) + \frac{\sqrt{\lambda^{St}}\beta}{\langle H^2_{DA}\rangle}u^2(\Delta A^{\neq})\right]$$

with $C = \dfrac{\hbar\sqrt{4\pi/\beta}}{2\pi} . \exp\left(\beta \Delta A^{\neq}\right)$,

$$u^2\left(\langle H_{DA}^2\rangle\right) = \frac{var(H_{DA}^2)}{\rho N},$$

and $u^2(\Delta A^{\neq})$ being also obtained from the uncertainty propagation formula, as follow.

$$\Delta A^{\neq} = \frac{(\Delta A^{\circ} + \lambda^{St})^2}{4\lambda^{St}} - \langle H_{DA}\rangle_1$$

$$u^2(\Delta A^{\neq}) = \frac{(\Delta A^{\circ} + \lambda^{St})}{4\lambda^{St}} u^2(\Delta A^{\circ}) + \frac{8(\Delta A^{\circ} + \lambda^{St})\lambda^{St} - 4(\Delta A^{\circ} + \lambda^{St})^2}{16(\lambda^{St})^2} u^2(\lambda^{St}) + \frac{var(H_{DA})}{\rho N}$$

ET transfers time from mean first passage

Technical details on BOMD simulations

We extracted 21 snapshots with a 2 ps time interval from the initial BOMD simulation on the resting state, before switching to cDFT/MM to simulate nuclear relaxation on the $(US)^+P$ potential energy surface. We used a 0.5 fs time step to have better time resolution of MD trajectory. MD simulations were carried out for a maximum 200 fs on the initial diabatic states. The vertical energy gap between the two diabatic states was evaluated in a second step with the POL3 water model using the procedure described above.

As it turned out that the hopping probability at the crossing point was very sensitive to the choice of XC functional, all the simulations (trajectory generation and reprocessing) were repeated with the following functionals: BH&HLYP, PBE50 (i.e. PBE0 with 50% of exact exchange), M06-2X, HSE06.

Characteristic decoherence times

Characteristic decoherence times have been evaluated from the difference in forces exerted on atom nuclei between the two charge transfer states $\tau_{dec} = \left[\left\langle\sum_n \dfrac{(F_{n,i} - F_{n,f})^2}{2 a_n \hbar}\right\rangle_T\right]$. The sum runs over all atom nuclei, and enable to make a separation between atom pertaining to the USP molecule, and those pertaining to solvent. Results are compiled in Sable S1

The parameters a_n are nuclear wave packet widths that we be borrowed from Ref except for phosphorous that was not considered in this work and that we have substituted here by a high temperature estimate ($a_P = 6M_P/\beta\hbar^2$, M_P being the atomic mass of phosphorous).

Table S1: Characteristic decoherence times (in fs) for the superposition of the (US)⁺P and (US)P⁺ diabatic states. The separation into an USP and solvent contribution is enabled with Eq. 6 (see main text).

	τ_{dec}^{all}	τ_{dec}^{USP}	$\tau_{dec}^{solvent}$
BH&HLYP	0.61	0.86	0.86
PBE50	0.60	0.85	0.84
M06-2X	0.64	0.94	0.87
HSE06	0.74	1.24	0.93